

Energy-dependent cross sections and nonadiabatic reaction dynamics in $F(^2P_{3/2}, ^2P_{1/2}) + n-H_2 \rightarrow HF(v, J) + H$

Sergey A. Nizkorodov, Warren W. Harper, William B. Chapman, Bradley W. Blackmon, and David J. Nesbitt^{a)}

JILA, University of Colorado and National Institute of Standards and Technology, and Department of Chemistry and Biochemistry, University of Colorado, Boulder, Colorado 80309-0440

(Received 1 June 1999; accepted 13 August 1999)

High-sensitivity direct IR laser absorption methods are exploited to investigate quantum state-resolved reactive scattering dynamics of $F + n-H_2(j=0,1) \rightarrow HF(v, J) + H$ in low-density crossed supersonic jets under single collision conditions. Nascent rotational state distributions and relative cross sections for reactive scattering into the energetically highest HF ($v=3, J$) vibrational manifold are obtained as a function of center-of-mass collision energies from $E_{\text{com}} = 2.4$ kcal/mole down to 0.3 kcal/mole. This energy range extends substantially below the theoretically predicted transition state barrier [$E_{\text{barrier}} \approx 1.9$ kcal/mole; K. Stark and H. Werner, *J. Chem. Phys.* **104**, 6515 (1996)] for the lowest *adiabatic* $F(^2P_{3/2}) + H_2$ potential energy surface, therefore preferentially enhancing *nonadiabatic* channels due to spin-orbit excited $F^*(^2P_{1/2})$ ($\Delta E_{\text{spin-orbit}} = 1.15$ kcal/mole) in the discharge source. The HF ($v=3, J$) cross sections decrease gradually from 2.4 kcal/mole down to the lowest energies investigated ($E_{\text{com}} \approx 0.3$ kcal/mole), in contrast with exact adiabatic quantum calculations that predict a rapid decrease below $E_{\text{com}} \approx 1.9$ kcal/mole and vanishing reaction probability by $E_{\text{com}} \approx 0.7$ kcal/mol. Further evidence for a nonadiabatic $F^*(^2P_{1/2})$ reaction channel is provided by nascent rotational state distributions in HF ($v=3, J$), which are $>2-3$ -fold hotter than predicted by purely adiabatic calculations. Most dramatically, the nascent product distributions reveal multiple HF ($v=3, J$) rovibrational states that would be *energetically inaccessible* from ground state $F(^2P_{3/2})$ atom reactions. These quantum state resolved reactive scattering studies provide the first evidence for finite nonadiabatic dynamics involving multiple potential energy surfaces in this well-studied “benchmark” $F+H_2$ reaction system. © 1999 American Institute of Physics. [S0021-9606(99)00242-1]

I. INTRODUCTION

The $F+H_2$ reaction system has represented an important focus of chemical dynamics research for several decades.¹⁻⁴ This reaction has several features that make it both particularly interesting and chemically challenging. First of all, it is highly exothermic [$\Delta E = 32.001(14)$ kcal/mol], which leads to subsequent energy dispersal into many vibrational and rotational states of the HF products. Indeed, this reaction leads to a highly vibrationally inverted HF ($v \leq 3$) product distribution, which has long been exploited as an efficient pumping mechanism for HF chemical lasers.⁵ Additionally, the reaction proceeds over a low activation barrier ($E_{\text{act}} \approx 1.6$ kcal/mole)⁴ and is therefore quite rapid under room temperature conditions. Most importantly, the presence of unpaired electrons in the F atom reagent results in multiple, closely spaced potential energy surfaces on which the reaction can proceed, asymptotically correlating with different projections of the total electron spin+orbital angular momentum along the intermolecular axis. This proves especially relevant in the present work, since in the Born-Oppenheimer approximation, only reactions that remain on the *lowest adiabatic* surface should be accessible at these

collision energies (Fig. 1).⁶⁻⁸ Thus, a detailed study of reactive cross sections versus center-of-mass collision energy can begin to elucidate the importance of *nonadiabatic* (i.e., multisurface) versus *adiabatic* (i.e., single surface) contributions to the reaction dynamics.

The body of existing experimental and theoretical knowledge about the $F+H_2$ system is extensive. From the experimental side, the temperature-dependent reaction rate constants,⁹⁻¹² Arrhenius activation energies,⁴ cross sections,¹³⁻¹⁸ and product partitioning of rotational/vibrational energy¹⁹⁻²⁴ are available from a number of sources. In particular, early “arrested relaxation” experiments in the Polanyi group^{2,19} played a major role in our understanding of the $F+H_2$ reaction, as well in developing extremely useful models of atom+diatom reaction dynamics, in general. Crossed molecular beam studies in the Lee group by Neumark *et al.*^{13,14,25} have provided an enormously rich source of experimental information about relative cross sections and vibrationally resolved HF product angular distributions at selected center-of-mass collision energies. More recently, Faubel, Toennies, and co-workers have succeeded in measuring improved differential cross sections for the $F+D_2$ isotopic variant of the reaction,²⁶⁻³² as well as for inelastic scattering of F atoms by both H_2 and D_2 ,^{15,33} with substantially enhanced energy and angular resolution. Based on a

^{a)}Electronic mail: djn@jila.colorado.edu

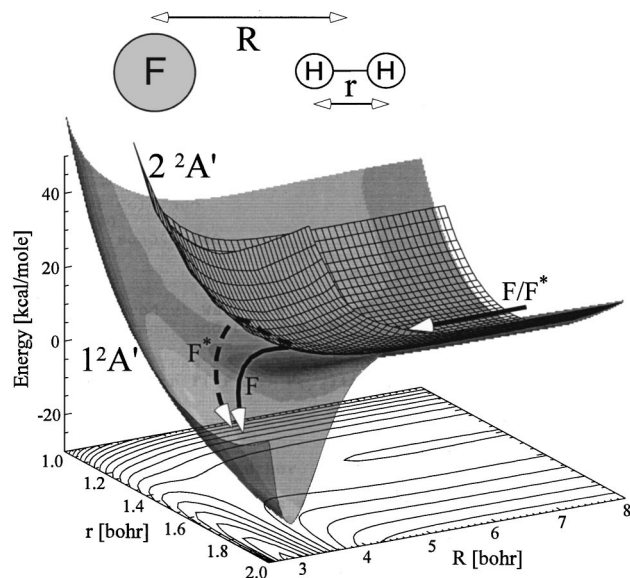


FIG. 1. Potential energy surfaces (PES) for a colinear reaction between F/H_2 and H_2 , plotted in Jacobi coordinates. Of the three low lying PES, two ($1^2A'$ and $1^2A''$) correlate to $F+H_2$ and one ($2^2A'$) to F^*+H_2 (only $1^2A'$ and $2^2A'$ PES are displayed). $F+H_2$ reactions (solid arrow) occur on $1^2A'$ PES (also shown as a contour plot), over an early 1.9 kcal/mole energy barrier. The $2^2A'$ surface is strongly repulsive, and thus F^*+H_2 collisions are predicted to be completely nonreactive in the *adiabatic* (i.e., Born–Oppenheimer) limit. However, some fraction of the F^*+H_2 encounters may result in a *nonadiabatic* crossing to the $1^2A'$ surface followed by the reaction (e.g., dashed arrow). The main thrust of the present work is to exploit nascent $HF(v,J)$ quantum state distributions as a function of E_{com} to experimentally identify and characterize these nonadiabatic processes.

clever alternative approach, $F+H_2$ reaction dynamics have also been studied in the Neumark group by photoelectron detachment studies of the FH_2^- anion, thereby directly accessing the FH_2 transition state region.^{34–36}

In the above beam studies, information on the reaction dynamics and final quantum state distributions is achieved by kinetic energy analysis of the product fragments, with a resolution limited by time-of-flight (TOF) methods. This level of resolution can readily distinguish product HF vibrational states ($\Delta E_{\text{HF}} \approx 4000 \text{ cm}^{-1}$), but is typically insufficient to achieve rotational state resolution ($B_{\text{HF}} \approx 20 \text{ cm}^{-1}$). A dramatic advance in $HF(v,J)$ quantum state resolution can be achieved by laser-based detection schemes. For example, shot noise limited direct IR absorption methods have been exploited in our group by Chapman *et al.*^{37,38} to study $F+H_2$ reaction dynamics in low-density, crossed supersonic molecular jets, rigorously yielding nascent $HF(v,J)$ product state distributions under collision-free conditions. The spectral resolution of these crossed jet direct absorption methods ($\Delta \nu_{\text{exp}} \approx 0.01 \text{ cm}^{-1}$) is over four orders of magnitude higher than TOF methods, resolving $HF(v,J)$ P or R branch transitions from adjacent rotational states by more than 4000-fold. Indeed, the laser resolution ($\Delta \nu_{\text{laser}} \approx 0.0001 \text{ cm}^{-1}$) in these studies is an additional two orders of magnitude below the Doppler limit, and therefore also contains information on lab frame velocity distributions of the $HF(v,J)$ product. In yet another development of combined laser and molecular beam methods, Keil and co-workers^{17,18} have succeeded in using

line tunable HF chemical lasers and optothermal detection to probe $HF(v,J)$ products from $F+H_2$ reactions. This offers the ability to obtain *differential* cross section information with full rovibrational quantum state resolution.

The list of theoretical studies on the $F+H_2$ system is perhaps even more impressive; the interested reader is referred to Refs. 1, 3, and 4 for an extensive historical discussion on the topic. One of the theoretical milestones of the last decade has been the calculation of a fully *ab initio* potential energy surface (PES) for $F+H_2$ by Stark and Werner (SW),^{39,40} claimed to be accurate to better than ± 0.2 kcal/mole for all relevant nuclear configurations. This should be contrasted with previous potential energy surfaces that were for the most part either purely empirical or contained empirical corrections optimized to reproduce existing experimental results.^{41–47} Classical and quantum-mechanical calculations performed on the SW PES were found to reproduce qualitatively (i) vibrationally resolved reaction differential cross sections,^{48–52} (ii) thermal rate constants,^{49,53} (iii) kinetic isotope effects,⁵³ (iv) rovibrationally resolved differential cross section results,^{17,51} as well as (v) nascent HF product state distributions.³⁸ Most importantly, a detailed photoelectron structure arising from transition state spectroscopy of FH_2^- was also correctly predicted,^{54,55} which was not possible with any other PES. Indeed, though some experimental results exist (such as the differential cross sections for inelastic $F+H_2/D_2$ scattering) for which semiempirical potential energy surfaces appear to perform as well or even better,³³ the Stark and Werner PES is widely considered to be the best currently available.

Despite this considerable progress, several fundamentally important theoretical and experimental questions remain. One issue that has received increasing attention in recent years concerns the interplay between spin–orbit excitation and nonadiabatic effects in the $F+H_2$ reaction dynamics.³ Atomic fluorine has two low lying spin–orbit states, $F(^2P_{3/2})$ and $F(^2P_{1/2})$ separated by only $\Delta E_{\text{spin-orbit}} = 1.15 \text{ kcal/mole}$,^{56,57} which will be designated throughout this paper as F and F^* , respectively. Though energetically small, this spin–orbit excitation is dynamically crucial, since the F^*+H_2 potential energy surface correlates with a strongly repulsive quartet state of the products (see Fig. 1). In the Born–Oppenheimer approximation, therefore, only the *lower* spin–orbit state F atom is predicted to be reactive with H_2 .⁸ Thus, the presence or absence of significant spin–orbit excited reaction pathways in such a system directly tests whether reactive collisions are constrained to a *single, adiabatic* potential surface or whether much richer and more complicated dynamical possibilities exist due to *nonadiabatic* interactions on *multiple* potential surfaces.

Many theoretical studies have predicted appreciable nonadiabatic effects in the $F+H_2$ reaction,^{58–79} though scatter in the estimate of these effects is large. For example, semiclassical treatments by Komornicki *et al.*^{63,64} show that cross sections for the nonadiabatic $F(^2P_{1/2})+H_2$ channel can be as high as 50% of those for the adiabatic $F(^2P_{3/2})+H_2$ channel, especially at higher collision energies. Similarly, Lepetit *et al.*⁶⁶ have found very significant nonadiabatic reaction probabilities using close-coupling calculations and hy-

perspherical potentials. In quasiclassical surface hopping studies of F^*+H_2 , Tully^{75,76} demonstrate the importance of the nonadiabatic reaction channel and the intimately related process of electronic quenching of F^* by collisions with H_2 . Gilbert and Baer, on the other hand, predict only a $\approx 1\%–2\%$ effect,^{61,62} though their results, as well as the calculations of Billing *et al.*,⁵⁹ do demonstrate sensitivity in the integral reaction cross sections to the single versus multiple potential surface nature of the theoretical treatment. More recently, Alexander *et al.*⁵⁸ have reported preliminary results on full quantum reactive scattering calculations for F/F^*+H_2 , including all three adiabatic surfaces from the *ab initio* work of Stark and Werner. Though only obtained for $J_{\text{tot}}=\frac{1}{2}$ and therefore not converged with respect to the partial wave expansion, these calculations do represent a rigorous, multisurface dynamical treatment of spin-orbit and Coriolis coupling effects, and predict overall reaction probabilities for the F^* channel to be small but significant. Specifically, Alexander *et al.* report nonadiabatic (F^*+H_2) versus adiabatic ($F+H_2$) reaction probabilities for forming HF in the $v_{\text{HF}}=3$ vibrational manifold on the order of 10% at $E_{\text{com}}\approx 2$ kcal/mole and, most importantly, dropping off much more slowly for F^* than F with center-of-mass collision energy below the adiabatic reaction barrier.⁵⁸

In rather surprising contrast with these theoretical predictions, there have been no experiments until quite recently that have unambiguously confirmed the presence of the nonadiabatic F^*+H_2 reaction channel.^{3,80} As clarified in this work, this is most likely the result of relatively modest nonadiabatic contributions predicted at collision energies near and above the reaction barrier as well as limited quantum state resolution in previous studies. A much more sensitive approach involves exploring the reaction at energies significantly *below* the adiabatic transition state barrier, where $F+H_2$ reactions can be sufficiently suppressed to permit nonadiabatic F^*+H_2 channels to predominate. Preliminary evidence for such nonadiabatic processes has been presented elsewhere, based predominantly on reactive scattering studies at $E_{\text{com}}\approx 0.54(10)$ kcal/mole.⁸⁰ Considerably more detailed information on nonadiabatic versus adiabatic reaction dynamics can be obtained by extending these studies over a much wider range of collision energies. Such an energy-dependent reactive scattering study forms the major thrust of this paper, based on fully quantum state resolved $HF(v,J)$ product distributions obtained over a range of $E_{\text{com}}\approx 2.4–0.3$ kcal/mole, i.e., from both above to substantially below the 1.9 kcal/mole barrier theoretically predicted for a reaction on the lowest potential energy surface.

II. EXPERIMENT

The crossed-jet reactive scattering apparatus has been described in detail elsewhere;³⁸ only a brief description and modifications relevant to the current study are mentioned here. Two pulsed molecular jets, one containing fluorine atoms formed in a pulsed discharge of F_2 /rare gas and the other supersonically cooled H_2 in rare gas mixtures, are crossed at right angles ≈ 4.5 cm downstream of the two nozzle orifices under low-density conditions. The $HF(v,J)$ products formed in the intersection region are probed with complete quantum

state resolution via direct IR absorption of a continuous-wave single-mode ($\Delta\nu\approx 0.0001\text{ cm}^{-1}$) F-center laser, multipassed 16–18 times through the jet intersection plane with a cylindrical Herriot cell. Absorption due to reactively formed $HF(v,J)$ is monitored by transient imbalance between signal and reference IR laser beams on matched InSb detectors, which is then sampled with a fast digitizer. Dual time gating ($\Delta t\approx 200\ \mu\text{s}$) of the signal before and during the gas pulse is used to further discriminate against noncommon mode noise on the signal beam due to low-frequency acoustic vibrations in the multipass cell.

The HF product states can be energetically formed in $v_{\text{HF}}=0,1,2,3$ and are probed by direct absorption on the fundamental ($\Delta v=+1$) bands between 3600–3900 cm^{-1} . For each $HF(v',J')\leftarrow HF(v'',J'')$ probe transition, the absolute absorbance of the laser is recorded as a function of laser frequency and integrated over the full Doppler profile (full scan ≈ 2500 MHz, 3 MHz step size), rigorously yielding the *absolute* column-integrated density difference between the upper and lower $HF(v,J)$ states. Since the $HF(v=4)$ manifold is unpopulated by both adiabatic and nonadiabatic F/F^*+H_2 reaction channels, the $v=4\leftarrow 3$ absorbance signals are readily related to the $HF(v=3,J)$ rotational populations. The infrared laser power is kept below 60 μW to ensure that the signals are in the linear (i.e., unsaturated) absorption regime; this is confirmed by detailed calculations and explicitly verified by power-dependent studies for the strongest HF transitions. Under these conditions, the single pulse experimental detection sensitivity is 3×10^{-7} per root Hz, corresponding to a rms absorbance of 3×10^{-5} in a ≈ 10 KHz detection bandwidth. Though already within a factor of 3–4 from the shot-noise limit, this can be further improved by signal averaging (2–4-fold) and integration over the full Doppler profile (10–20-fold). This degree of detection sensitivity proves essential for collision-free detection of the most weakly populated HF products, which as a result can be observed down to concentrations $\approx 10^7–10^8$ molecules/ cm^3 /quantum state.³⁸

The hydrogen jet is generated by a piezoelectric transducer (PZT) pulsed valve based on the design of Proch and Trickl⁸¹ with argon/hydrogen mixtures maintained at a total backing pressure of 900 Torr. The mole fraction of Ar with H_2 is varied from 0% to 40% to vary the H_2 jet speed and thereby the center-of-mass collision energy between F and H_2 . The H_2 valve produces near-rectangular, 450 μs wide gas pulses with a rise/fall time of roughly 30 μs , as monitored in vacuum with a miniature hearing-aid microphone. The effective nozzle diameter is determined to be $145\pm 5\ \mu\text{m}$ from mass flow rate measurements; this agrees quite well with the actual nozzle diameter of 150 μm , confirming that the valve is fully open during the pulse. Under these H_2 backing pressure conditions and nozzle diameter, the total column-integrated density of H_2 4.5 cm away from the nozzle is $\approx 1.0\times 10^{14}\text{ cm}^{-2}$, corresponding to a density of $\approx 2.1\times 10^{13}\text{ cm}^{-3}$ in the intersection region. Based on a total reactive cross section of $\approx 3\ \text{\AA}^2$, the reaction probability per F atom is less than 3%, which makes the probability of secondary reactive encounters negligible.

The fluorine atoms are produced in a pulsed slit

(300 $\mu\text{m} \times 5$ mm) discharge source described in detail in Ref. 38. Two different mixtures containing fluorine have been used in present work, (i) 5% $\text{F}_2/95\%$ He and (ii) 5% $\text{F}_2/20\%$ Ne/75% Ar. The two expansion conditions yield two F atom velocities, i.e., “fast” [1.48(15) km/s] and “slow” [0.59(6) km/s], which, in conjunction with Ar doping of the H_2 jet, conveniently result in two partially overlapping ranges of center-of-mass collision energies ($E_{\text{com}} = 0.3\text{--}1.7$ kcal/mole and $1.0\text{--}2.4$ kcal/mole). To initiate and sustain the discharge, a negative pulse of ≈ -700 V is applied across the expansion in a 500–700 μs time window centered on the much longer (≈ 2 ms) total gas pulse. Typical discharge backing pressures range from 30 to 70 Torr, with peak discharge currents from 100 to 500 mA. Under these backing pressure conditions, both gas mixtures result in a smooth, stable discharge producing roughly comparable densities of fluorine atoms, as directly monitored by the HF absorption signals. The total column-integrated density of the F atom source jet (including the 20-fold excess of rare gas carrier) is less than $2 \times 10^{14} \text{ cm}^{-2}$, with an estimated number density of $\leq 5 \times 10^{13} \text{ cm}^{-3}$ in the intersection region. Based on a 5% fractional F_2 concentration in the discharge mixture and an assumed $\approx 5\%$ dissociation efficiency, this corresponds roughly to $\approx 10^{11} \text{ cm}^{-3}$ of F/F* atoms. The partitioning between F* and F atoms in the jet discharge is unfortunately not possible for us to measure with the current apparatus. However, based on the temperature and collision frequency in the discharge region, one might anticipate the relative fraction of F:F* to be close to the statistical limit of 4:2.

The primary focus of the present study is to measure state-resolved cross sections for reactively forming HF ($v=3, J$) as a function of collision energy. The rotational distributions of the HF ($v=3, J$) products are first established at two reference collision energies, specifically for neat H_2 expansions colliding with “slow” ($\text{F}_2/\text{Ne}/\text{Ar}$) and “fast” (F_2/He) fluorine atoms. The rotational distributions are then measured at a series of other collision energies by varying the Ar/ H_2 mixture (for both fast or slow F atom sources), with each data point referenced to the corresponding signals obtained under neat H_2 conditions. This offers a crucial advantage of permitting data to be compared quantitatively over many hundreds of hours of data collection, which typically exceeds time between routine maintenance of the discharge source. At such high detection sensitivity, extremely weak background absorption can be observed due to trace HF impurities excited in the F_2 discharge. However, the magnitude of this background is quite small (typically $\leq 10\%$ of the reactively formed HF signals) and readily compensated for by background scans in the absence of the H_2 reagent jet.

III. CENTER-OF-MASS COLLISION ENERGIES

The center-of-mass collision energy distribution, $P(E_{\text{com}})$, plays an important role in the discussion of the present data. In a conventional crossed-beam experiment, the width of the $P(E_{\text{com}})$ distribution is normally limited by the spread in reactant speeds; for crossed-jet reactive scattering

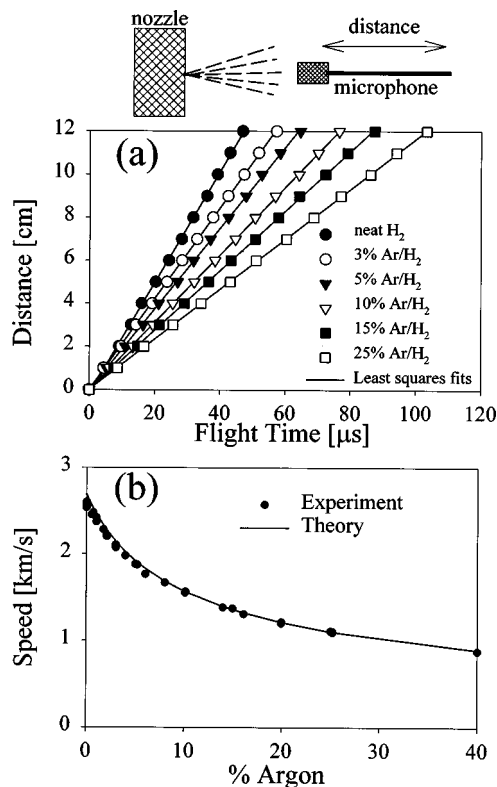
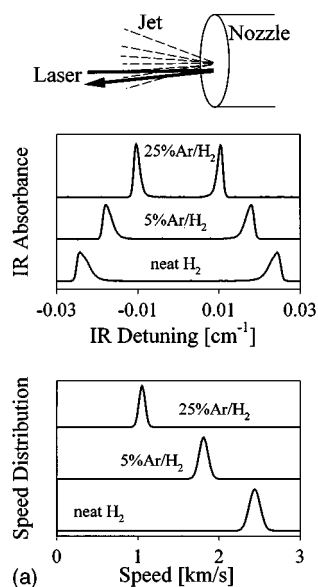


FIG. 2. Schematic for measuring centerline jet speeds with the TOF method. (a) Nozzle–microphone separation versus arrival time of the gas pulse is displayed for a series of Ar/ H_2 mixtures; the jet speeds are given directly by the slopes. (b) Speeds of Ar/ H_2 mixtures are plotted versus the percentage of added Ar. The dots represent experimental measurements, which agree extremely well with predictions (solid line) obtained from an ideal continuous isentropic expansion. The small deviations between theory and experiment are due to incomplete rotational cooling of H_2 .

studies, it is the angular distribution of the two jets that plays the more important role. Two independent methods have been developed to obtain these jet parameters, which will be briefly summarized here and described elsewhere in more detail.⁸² The first is based on monitoring the TOF profile of the gas pulse with a small hearing aid microphone as a function of the distance parallel and perpendicular to the jet expansion axis. The mean jet speed is simply obtained by translating the microphone along the jet axis and monitoring the gas pulse arrival time as a function of the nozzle–microphone separation (Fig. 2). The robust reliability of this method can be gauged from the linearity of the individual TOF curves [Fig. 2(a)], as well as from the small relative scatter of speeds for various Ar/ H_2 mixtures plotted in Fig. 2(b). As described elsewhere,⁸² these speed data agree quantitatively with detailed predictions of an adiabatic expansion model for Ar/ H_2 mixtures, i.e., explicitly taking into account (i) additional energy release from rotational cooling and (ii) temperature-dependent heat capacities of the *o*- H_2 , *p*- H_2 and Ar constituents.

The second method relies on high-resolution laser Dopplerimetry, accomplished by seeding trace amounts of an IR absorber (e.g., CH_4) into the expansion mix and recording Doppler profiles of a single rovibrational transition for different orientations of the laser beam with respect to the jet

Doppler Speed Measurements



Doppler Divergence Measurements

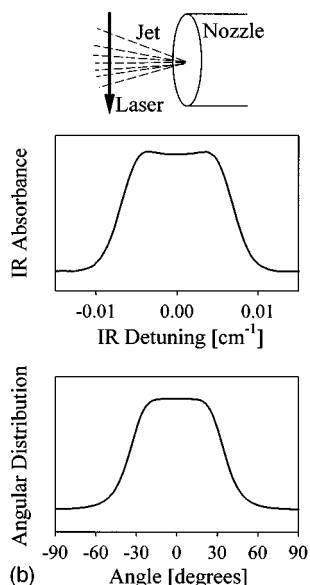


FIG. 3. High-resolution laser Dopplerimetry for measurements of supersonic jet speed and angular divergence. (a) The top panel shows scans over the individual absorption lines of methane seeded into three different Ar/H₂ mixtures. Because of the parallel detection geometry, each individual CH₄ absorption line is split into a doublet, with the splitting and the width of each feature providing information on the average and the width of the speed distribution, respectively. The bottom panel shows least squares fits for the corresponding speed distributions. (b) The concept is quite similar to that in (a), except that in this perpendicular probe arrangement the absorption profile (top) is determined primarily by the *angular* rather than speed distributions of the jet-cooled molecules (bottom).

axis [see Figs. 3(a) and (b)]. For laser propagation *parallel* to the jet axis [Fig. 3(a)], the absorption peak splits into two symmetric features, the separation and width of which are closely related to the average and width of the speed distribution. For laser propagation *perpendicular* to the jet axis [Fig. 3(b)], the Doppler profiles are broadened by and therefore most sensitive to angular divergence in the jet. These two Doppler profiles can be directly inverted to yield both

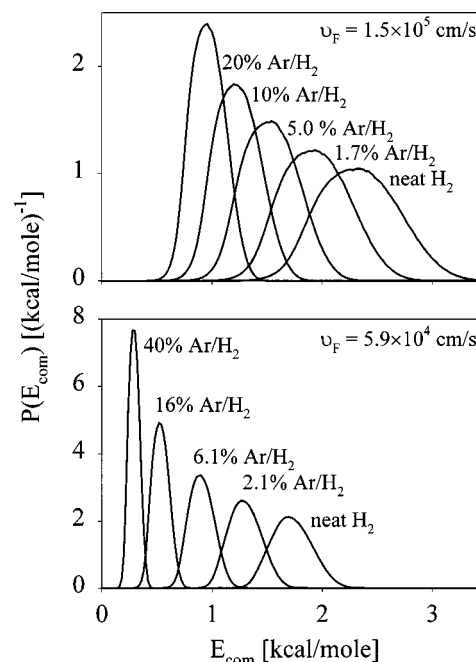


FIG. 4. Monte-Carlo simulation of the collision energy distributions. The top and bottom panel show the results for the “fast” [$1.48(15) \times 10^5$ cm/s] and “slow” [$5.9(6) \times 10^4$ cm/s] F-atom jets, respectively, colliding with different dilutions of Ar/H₂ mixtures. The range of collision energies covered in this experiment is from 2.4(5) kcal/mole down to 0.31(7) kcal/mole, where the width of the distributions is dominated by angular divergence of the jets. Collision energies quoted in the text correspond to averages over these Monte-Carlo distributions.

the angular and speed distributions of the IR chromophore,⁸⁰ sample data from which are shown in Fig. 3. It is worth noting that the speed and the angular jet divergence obtained from these more detailed Dopplerimetry measurements are in excellent agreement with the much simpler microphone based studies mentioned above.

With these jet speed and angular distributions established, $P(E_{\text{com}})$ is calculated from a Monte-Carlo simulation. This is accomplished by integrating over the jet intersection volume and the known speed and angular distributions for the F and H₂ jets, with each collisional event appropriately weighted by the local reagent densities (ρ_{H} , ρ_{F}), the relative velocity (v_{rel}), and the time spent in the probe laser beam. This additional weighting by time in the probe beam explicitly reflects the fact that a direct absorption method measures column-integrated *densities* rather than *fluxes* of HF(v, J) products, i.e., the density to flux transformation. Sample distributions for the crossed jet apparatus are presented for a series of collision energies in Fig. 4. Mostly as a result of favorable kinematics, the shapes of these $P(E_{\text{com}})$ distributions are fortunately quite insensitive to variations in the final quantum state of the HF($v=3, J$) product,³⁸ details of the reaction differential cross section, and translational temperatures of the jets.

Table I lists the jet speed combinations used in the experiment along with the first moments of the corresponding $P(E_{\text{com}})$ distributions. It is worth noting that the average values of E_{com} are about 10%–20% higher than energies predicted for a perpendicular jet intersection geometry. This

TABLE I. Relative integral cross sections for $F + n\text{-H}_2 \rightarrow \text{HF}(v=3) + \text{H}$ reactions. The first and third columns give the centerline speeds for the F and Ar/H₂ jets and the second column provides the amount of Ar seeded into the Ar/H₂ jet. E_{com} is the average collision energy of the $P(E_{\text{com}})$ distribution followed by its HWHM in parentheses. The “fast” and “slow” F atom jet cross section data have been scaled for best agreement in the region of overlapping collision energies, with 95 confidence intervals in parentheses.

v_F (km/s)	% Ar in Ar/H ₂	v_{H_2} (km/s)	E_{com} (kcal/mol)	σ (arb. units)
1.48(15)	0.0	2.58	2.35(46)	1.000(25)
"	0.7	2.44	2.17(44)	0.942(22)
"	1.7	2.26	1.95(41)	0.849(23)
"	3.0	2.09	1.75(37)	0.762(47)
"	5.0	1.89	1.54(33)	0.655(16)
"	8.0	1.67	1.33(29)	0.638(36)
"	10.0	1.56	1.24(27)	0.523(23)
"	14.0	1.39	1.10(24)	0.468(21)
"	19.9	1.21	0.98(21)	0.409(16)
0.59(6)	0.0	2.58	1.74(23)	0.810(33)
"	1.0	2.38	1.50(21)	0.707(65)
"	2.1	2.21	1.31(19)	0.570(33)
"	4.0	1.99	1.08(16)	0.421(37)
"	6.1	1.80	0.91(14)	0.352(32)
"	10.1	1.55	0.71(12)	0.250(17)
"	16.1	1.32	0.54(10)	0.195(22)
"	25.0	1.10	0.42(8)	0.187(42)
"	40.0	0.89	0.31(7)	0.186(22)
"	40.0	0.89	0.31(7)	0.151(30)

is due to a combination of (i) near-isoergic formation of the HF($v=3$) product and (ii) “heavy+light–light” F+H₂ kinematics. In essence, the HF product velocities in the laboratory frame are close to those of F atoms in the jet, altered only by the modest chemical energy release and the resulting small kick due to light hydrogen atom recoil. Thus, the majority of reactive collisions between F and H₂ resulting in HF($v=3, J$) signals occur for slightly *obtuse* angles, ≤ 1 cm prior to the probe laser region, which from the detailed Monte-Carlo simulations yields a slight upward shift in the average collision energy. As a final test, we have also performed these Monte Carlo calculations of $P(E_{\text{com}})$ for different angular spreads in the H₂ and F atom jets, in an effort to account for possible uncertainties in the jet angular divergence that might arise from seeding the expansion with Ar. As expected, these simulations indicate a completely negligible sensitivity to angular divergence of the F atom, due to the kinematic issues described above. Also, as expected, there is some sensitivity of $P(E_{\text{com}})$ to the H₂ jet divergence. However, the incremental effects on the average E_{com} due to any further increase in this width is rather small, on the order of 10%–20% for as much as an additional doubling of the jet divergence.

IV. RESULTS AND ANALYSIS

High resolution absorbance scans have been obtained over a sequence of HF rovibrational transitions [$v=4 \leftarrow 3; R(0)–R(6)$] for 18 collision energies between $E_{\text{com}} = 0.3$ and 2.4 kcal/mole. Sample HF Doppler profile data for $R(0)$ through $R(6)$ at four representative collision energies are shown in Fig. 5 and immediately indicate several points worth noting. First of all, the raw peak absorbance to rms

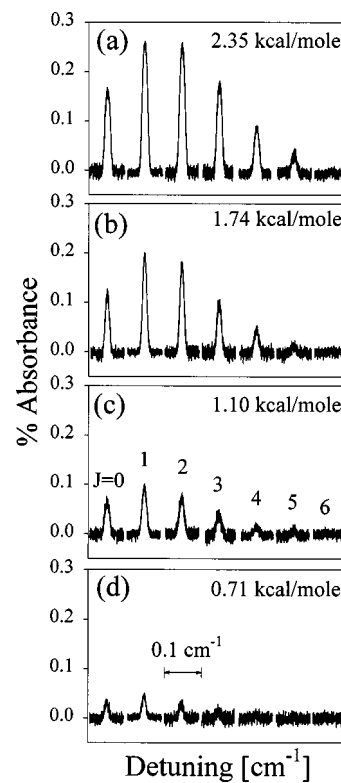


FIG. 5. Sample nascent HF absorbance data on individual R -branch $v=4 \leftarrow 3$ transitions at four representative collision energies. (a) 2.35(46) kcal/mole (“fast” F+neatH₂); (b) 1.74(23) kcal/mole (“slow” F+neatH₂); (c) 1.10(24) kcal/mole (“fast” F+14%Ar/H₂); and (d) 0.71(12) kcal/mole (“slow” F+10%Ar/H₂). Absorbance data have been obtained for a range of 18 collision energies and are used to extract state-resolved nascent HF($v=3, J$) populations as a function of E_{com} (see the text for details).

noise ratios are approximately 30:1 for the most intense transitions, which are further enhanced by an additional 10-fold from integration over the Doppler profile. As a result, the uncertainties in the HF state-to-state cross sections reported herein [i.e., $\approx 3\%–10\%$ with respect to the cross section formation of HF($v=3, J=1$) at $E_{\text{com}}=2.35$ kcal/mole] are independent of peak absorption signal strength for all but the very lowest collision energies. Furthermore, as a result of modest kinetic energy release in the HF($v=3$) manifold [i.e., $m_{\text{HF}}/(m_{\text{H}}+m_{\text{HF}}) \approx 95\%$ of this excess energy is kinematically removed by light H atom recoil], the Doppler widths are dominated by angular divergence in the jet and therefore only weakly dependent on the final product quantum state. Thus, the qualitative trends in nascent populations can be directly estimated from the peak absorption intensities, which, in turn, depend strongly on quantum state. Specifically, there is a clear peaking of the signal strengths at low J values, with a systematic decrease with increasing rotational state up to the energetic limit (i.e., $J \approx 6$ for $E_{\text{com}} = 2.35$ kcal/mole).

Since no products are formed in the HF($v=4$) vibrational manifold, the column-integrated densities of the nascent HF($v=3, J$) can be rigorously obtained from the measured integrated absorbances, according to

$$\int A(\nu) d\nu = \frac{8\pi^3\nu_0|m|\mu^2}{3hc(2J''+1)} \times \int [\text{HF}(v=3,J'')] dl, \quad (1)$$

where ν_0 is the transition center frequency, $m=J''+1$ ($-J''$) for R-branch (P-branch) transitions, and μ is the transition dipole moment given in Ref. 83. As discussed in detail in previous work,^{38,80} the ‘‘heavy+light–light’’ kinematics for $\text{F}+\text{H}_2$ results in an essentially flat density to flux transformation, especially so for the nearly isoergic formation of the $\text{HF}(v=3)$ manifold. Indeed, detailed Monte-Carlo simulations indicate that the integrated signal absorbances are directly proportional to state-resolved integrated product fluxes at any given collision energy and for all product HF quantum states to better than 5%–10% accuracy. In order to obtain relative cross sections as a function of collision energy, however, one must scale for additional effects due to (i) relative velocity and (ii) mole fraction of H_2 in the Ar/H_2 expansion mixture, both of which are varied in order to tune E_{com} . The relative integral cross sections into a given final J state are therefore calculated from

$$\sigma_j(E_{\text{com}}) \propto \frac{\int [\text{HF}(v=3,J)] dl}{X\sqrt{E_{\text{com}}}}, \quad (2)$$

where X is the mole fraction of H_2 in the H_2/Ar mixture. As described in Sec. II, all integrated absorbances and reaction cross sections are measured with respect to fixed reference collision energy conditions, i.e., for a jet expansion of neat hydrogen ($X=1$). Since the absolute F atom populations in the jet intersection region are not measured in the current experiment, the data obtained under the two discharge conditions (i.e., ‘‘fast’’ and ‘‘slow’’ fluorine jets) are treated independently, and then scaled with a single parameter in the region of overlapping collision energies ($E_{\text{com}} \approx 1.0$ – 1.7 kcal/mole).

The relative cross sections for forming $\text{HF}(v=3,J)$ as a function of rotational state J are presented in Fig. 6 over a sample range of collision energies, which demonstrates several interesting trends. First of all, the reaction cross sections decrease smoothly and systematically as a function of collision energy. Second, despite a more than fourfold change in collision energy, the cross sections into a given final J state rise and fall in a qualitatively similar manner. On closer inspection, some sensitivity to collision energy becomes evident, with the most probable rotational state of $\text{HF}(v=3)$ systematically shifting toward lower J values with decreasing E_{com} . For example, the maximum of the $\text{HF}(v=3,J)$ distribution shifts from $J=2$ at $E_{\text{com}} \approx 1.8$ kcal/mole to $J=1$ at lower collision energies ($E_{\text{com}} \leq 1.5$ kcal/mole). Substantially more surprising, however, is the relatively modest sensitivity of a reaction cross section to the center-of-mass collision energy. Specifically, one might have expected a sharp decrease in the reaction cross section at energies lying below the theoretical transition state barrier predicted at ≈ 1.9 kcal/mole. Instead, a significant yield of HF products is observed down to $E_{\text{com}} \approx 0.3$ kcal/mol, i.e., the lowest collision energy of the present experiment. This point is explicitly addressed in Fig. 7, where the total $v_{\text{HF}}=3$ reactive cross sections (i.e., summed over all rotational states) are plotted as a function of E_{com} (see also Table I). The cross sections do

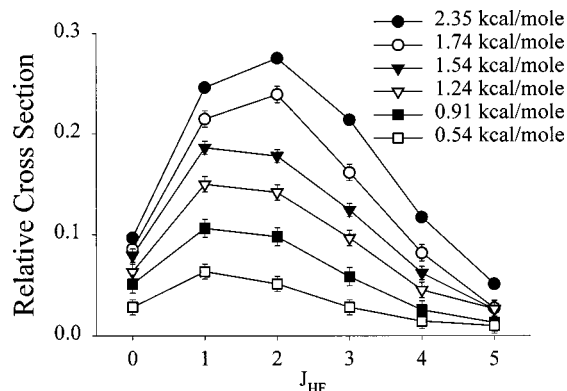


FIG. 6. Relative state-resolved reaction cross sections for $\text{HF}(v=3,J)$ for several collision energies. The cross sections decrease smoothly with E_{com} for every $\text{HF}(v=3,J)$ state, with a slight shift in the peak of the nascent distribution from $J \approx 2$ to $J \approx 1$. Especially noteworthy is the quite modest (≈ 2.5 -fold) decrease in the cross section for collision energies up to 1 kcal/mole below the ≈ 1.9 kcal/mole barrier height predicted for adiabatic $\text{F}+\text{H}_2$ reactions.

decrease monotonically with decreasing collision energy, but there is little evidence for an energetic threshold below 1.9 kcal/mole due to the adiabatic transition state barrier. This unexpected shape of $\sigma(E_{\text{com}})$ will be discussed more fully in the context of detailed theoretical predictions in the next section.

V. COMPARISON WITH THEORY

As a prelude to the present energy-dependent studies, nascent $\text{F}+\text{H}_2$ distributions have been investigated for $\text{HF}(v,J)$ products in each of $v_{\text{HF}}=0,1,2,3$ rovibrational manifolds.³⁸ Though only obtained at a single center-of-mass

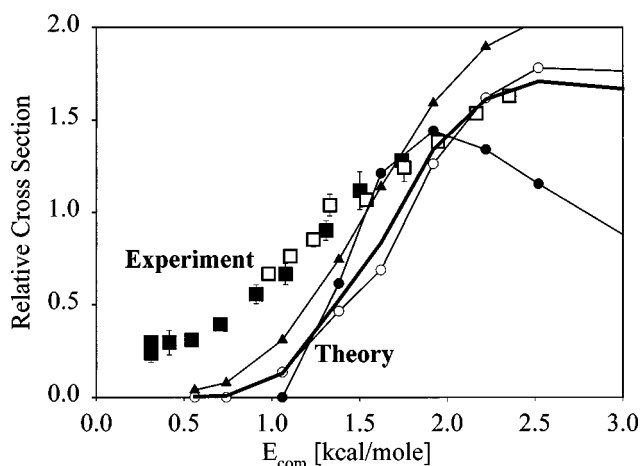


FIG. 7. Total HF reactive cross sections into $v=3$ (i.e., summed over all final J) as a function of collision energy, E_{com} . The ‘‘fast’’ F-jet data (large open squares) and the ‘‘slow’’ F-jet data (large filled squares) are analyzed independently and scaled to each other in the overlapping E_{com} range. The theoretical curves reflect quantum mechanical scattering calculation on SW PES for $\text{F}+\text{H}_2(j)$: $j=0$ (filled circles); $j=1$ (open circles); $j=2$ (triangles). Also presented is the theoretical prediction for $n\text{-H}_2$ at 200 K (thick solid line). As discussed in the text, the theoretical calculations have been shifted by $1/3\Delta E_{\text{spin-orbit}}=0.38$ kcal/mole to higher energy to account for the increase in barrier height when spin-orbit effects are incorporated. The experimental data are in relative units while the theoretical cross sections are reported in \AA^2 .

collision energy $E_{\text{com}}=2.4$ kcal/mole, this nevertheless has allowed a first rigorous state-to-state comparison with “exact” (i.e., fully converged) quantum calculations on the lowest *ab initio* potential surface of Stark and Werner. These direct comparisons have proven qualitatively very successful in modeling the overall rovibrational distributions observed experimentally, but also indicate significant discrepancies, especially for states in the highest HF ($v=3, J$) vibrational manifold. Consequently, the current study has focused explicitly on the $v_{\text{HF}}=3$ manifold, yielding first quantum state resolved cross sections for HF ($v=3, J$) formation over a broad range of collision energies, including those sampling substantially *below* the adiabatic reaction barrier for F+H₂ reactions. These energy-dependent data permit an even more demanding comparison between experiment and theory, as discussed below.

Arguably the best F+H₂ reactive scattering calculations (and most relevant to our experimental conditions) have been performed by Castillo *et al.*^{52,84} on the fully *ab initio* potential energy surface of Stark and Werner (SW PES).⁵⁹ In these studies, the reaction has been treated *adiabatically* on the lowest-energy $1^2A'$ PES, i.e., without including any spin-orbit effects. The calculations provide fully converged differential and integral state-resolved cross sections at a series of center-of-mass collision energies especially well suited for a comparison with the present experimental results.

Theoretical studies agree that the spin-orbit interaction can have a twofold effect on the F+H₂ reactive scattering dynamics.³ First of all, the spin-orbit interaction raises the reaction barrier on the lowest adiabatic $1^2A'$ PES by approximately one-third the F atom spin-orbit splitting, i.e., from 1.54 kcal/mole to about 1.9 kcal/mole.⁵¹ Second, it contributes to the non-Born Oppenheimer, derivative coupling between the low-lying zeroth-order PES's, increasing the probability of *nonadiabatic* reactions between F* with H₂.³ Fully converged quantum-mechanical calculations on multiple PES's with rigorous treatment of nonadiabatic and spin-orbit effects will ultimately be necessary to obtain the most accurate picture of the reaction dynamics. *Multisurface* calculations for atom+diatom reactive scattering represent a state-of-the-art challenge in the field, and in the F/F*+H₂ reaction system have thus far only been performed⁵⁸ for the lowest value of total angular momentum, $J_{\text{tot}}=\frac{1}{2}$. Nevertheless, these initial results already have provided useful insights into the influence of spin-orbit excitation on the effective barrier height. Specifically, the studies indicate that the ground state $F(^2P_{3/2})+H_2(j=0)$ integral cross sections exhibit similar energy dependence as calculated for the uncorrected PES, provided that the collision energy is referenced *with respect to the transition state barrier*.^{51,84} Thus, until more detailed multiple surface results for the spin-orbit corrected PES become available, the best theoretical estimate of the adiabatic energy-dependent cross sections is obtained from the extensive adiabatic calculations already performed for the *spin-orbit uncorrected* PES, shifting the collision energy axis upward by the 0.38 kcal/mole change in barrier height. It is worth stressing that we anticipate rapid theoretical progress in this direction, such that direct comparisons will be possible in the near future as calculations fully con-

verged with respect to total angular momentum become available.

The F+H₂($j=0,1,2$)→H+HF($v=3$) integral reactive cross sections of Castillo *et al.*⁸⁴ are plotted in Fig. 7 against collision energy, which per the above discussion has been approximately corrected for spin-orbit effects by a 0.38 kcal/mole energy shift. The theoretical cross sections are also plotted for a *n*-H₂ at 200 K, consistent with expected rotational distribution of H₂ in the jet. The experimental cross sections have been normalized by a single parameter to match the theoretical *n*-H₂ data for the highest energies sampled ($E_{\text{com}}\approx 1.9$ –2.4 kcal/mole), i.e., where the calculations are expected to depend least on details of the potential surface, such as barrier widths, quantum tunneling contributions, etc. Qualitatively, the theoretically predicted and experimentally observed cross sections both exhibit a monotonic decrease with E_{com} ; however, the quantitative agreement with theory is rather poor. Specifically, theory suggests vanishingly small reactivity below $E_{\text{com}}\approx 1$ kcal/mole, whereas significant HF ($v=3, J$) product yields are observed in the experiment down to $E_{\text{com}}\approx 0.3$ kcal/mole. The experimental results suggest additional HF(v, J) contributions from a lower threshold channel not accounted for by purely adiabatic calculations on the ground spin-orbit F+H₂ surface.

It is interesting to note that quantum tunneling in the F+H₂ system is clearly quite important at these lower energies, which can be immediately recognized, since even the *theoretically* predicted cross sections extend well *below* the 1.9 kcal/mole reaction barrier. Thus, based on the well-known exponential sensitivity of tunneling effects, one might be justifiably concerned that any discrepancies between theory and experiment might be simply due to relatively small errors in the potential surface near the transition state geometry. We return to this important point in Sec. VI, where threshold studies have been performed to explicitly eliminate this possibility by identifying HF ($v=3, J$) quantum states that are energetically inaccessible to purely adiabatic reactions on the ground spin-orbit state surface.

Additional evidence for nonadiabatic contributions to the reaction dynamics is found in the HF product state distributions themselves. As shown in Fig. 8, for example, the average rotational energy $\langle E_{\text{rot}} \rangle$ of products formed in HF($v=3$) is found to be in relatively poor agreement with theory. Specifically, the average HF ($v=3, J$) rotational energy is theoretically predicted to monotonically decrease with E_{com} and essentially vanish for F+H₂($j=1$) below $E_{\text{com}}\approx 0.7$ kcal/mole. In contrast, the experimental $\langle E_{\text{rot}} \rangle$ values are 2–3-fold larger than predicted, with only modest (20%) fractional changes observed over the entire range of $E_{\text{com}}\approx 0.3$ –2.4 kcal/mole. Interestingly, the theoretical curves appear to lie systematically *lower* than the experimental data points by ≈ 0.2 –0.3 kcal/mole, which is close to the amount (≈ 0.2 kcal/mole^{3,39}) by which the SW PES is known to underestimate the $F(^2P_{3/2})+H_2$ reaction exothermicity. However, it would appear dynamically quite unlikely for this excess energy to be channeled exclusively into rotational energy of the HF($v=3$) products. The data therefore suggest

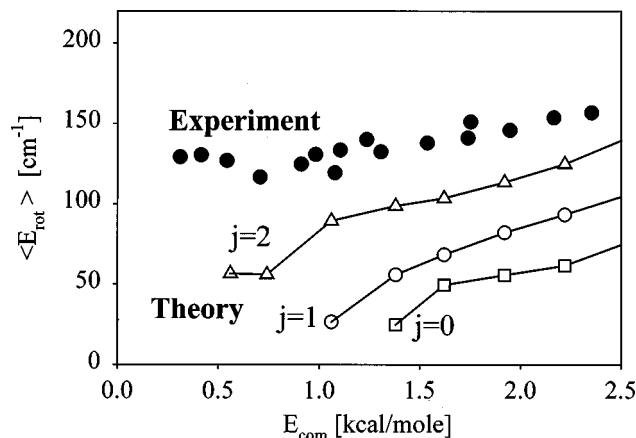


FIG. 8. Average rotational energy released into HF($v=3$) product state, calculated via $\langle E_{\text{rot}} \rangle = \sum_j \{ \sigma(J) \times E_{\text{rot}}(J) \} / \sum_j \sigma(J)$, where $\sigma(J)$ is the relative cross section for forming HF ($v=3, J$). The theoretical curves are fully converged QM scattering results on the SW PES. As discussed in the text, the theoretical E_{com} values have been shifted to higher energy by $1/3\Delta E_{\text{spin-orbit}} = 0.38$ kcal/mole to account for the increase in barrier height when spin-orbit splitting effects are incorporated. Note that the nascent HF($v=3$) products are formed with substantially (2–3-fold) more rotational energy than predicted by adiabatic theory.

some additional source of energy in the reagents that ultimately appears in the HF ($v=3, J$) products.

A plausible first suspect for this source of excess energy would be contributions from rotationally excited hydrogen, which due to a large rotational constant ($B \approx 60 \text{ cm}^{-1}$) is well known for its reluctance to cool in an expansion. The situation is further aggravated by ortho–para nuclear spin statistics, which preclude $\Delta j \neq 1$ transitions and thus require even larger energy changes [$\Delta E(j=2 \rightarrow 0) \approx 360 \text{ cm}^{-1}$ and $\Delta E(j=3 \rightarrow 1) \approx 600 \text{ cm}^{-1}$] to relax rotationally. On the other hand, this anomalously large B constant also constrains the initial rotationally excited populations in the stagnation region. Specifically, even at 300 K, $\geq 80\%$ of $n\text{-H}_2$ resides in the lowest para ($j=0$) and ortho ($j=1$) states, thus providing a rigorous *upper* limit on rotationally excited $\text{H}_2(j \geq 2)$ populations in the expansion. The H_2 reagent jet is actually substantially colder than this worst case estimate. For example, previous beam studies in neat H_2 expansions indicate that for comparable backing pressure \times orifice diameter conditions ($p_0 \times d \approx 13 \text{ Torr cm}$), the rotational distributions are best characterized by a temperature of $\approx 200 \text{ K}$.^{85–88} Furthermore, the current data is predominantly obtained with Ar/ H_2 mixtures, in which rotational relaxation is expected to be considerably more efficient. In any event, an upper limit of 200 K already translates into $\geq 90\%$ population in $\text{H}_2(j=0,1)$.

As described elsewhere,^{80,82} an independent confirmation of $\approx 200 \text{ K}$ temperature estimate for neat $n\text{-H}_2$ expansions is obtained in our apparatus by comparing measured and predicted jet speeds with an adiabatic expansion model that explicitly treats rotational cooling and temperature-dependent heat capacities of $n\text{-H}_2$. In addition, this analysis also provides evidence for preferential cooling of $n\text{-H}_2$ in Ar-doped expansion mixtures, with rotational temperatures as low as $\approx 100 \text{ K}$. This last point is particularly important,

since the most significant discrepancies between theory and experiment are observed at the lowest collision energies, which are obtained in $n\text{-H}_2$ mixtures with the greatest Ar mole fraction ($X_{\text{Ar}} \approx 20\% - 40\%$). As a result, $T_{\text{rot}} \leq 200 \text{ K}$ can be considered as a very safe upper limit for all Ar/ H_2 mixtures employed in the present study, which translates into $\leq 10\%$ rotationally excited $n\text{-H}_2$ in $j \geq 2$.

Furthermore, for such a small fraction of reagent H_2 ($j \geq 2$) to account for these population discrepancies would require an extreme sensitivity in the $\text{F} + \text{H}_2(j)$ reaction cross section to an initial H_2 rotational state. However, the theoretical calculations do not indicate such a sensitivity. For example, Fig. 7 reveals that at $E_{\text{com}} \leq 2 \text{ kcal/mol}$ the theoretical $\text{F} + \text{H}_2(j)$ integral cross sections drop with decreasing energy at roughly comparable rates for $j=0, 1$, and 2.⁸⁴ Indeed, the $\text{F} + \text{H}_2(j=0)$ cross section predominates around $E_{\text{com}} = 1.5 \text{ kcal/mole}$, suggesting that H_2 rotation is not as efficient as translation in terms of promoting a chemical reaction. Though the reaction *thresholds* in Fig. 7 do shift to lower E_{com} for higher j , the calculated $\text{F} + \text{H}_2(j=2)$ cross sections below $E_{\text{com}} = 1 \text{ kcal/mole}$ are far too small to account for the experimental observation. Indeed, even a *pure* beam of $\text{H}_2(j=2)$ would not be sufficient to make the present experimental results compatible with the adiabatic $\text{F} + \text{H}_2(j)$ predictions of Castillo *et al.*

To explicitly demonstrate the lack of influence of H_2 rotational relaxation on the experimental cross sections, the low E_{com} measurements have been repeated under different Ar/ H_2 expansion conditions, with $p_0 \times d$ ranging from 5 to 20 Torr cm. According to the data of Pillard *et al.*,⁸⁵ this would translate into a decrease in the $\text{H}_2(j \geq 2)/\text{H}_2(j \leq 1)$ ratio by a factor of 2 for a neat hydrogen expansion. The magnitude of this effect would be expected to be even larger for the Ar-doped mixtures used herein to achieve low E_{com} . Within experimental uncertainty, neither the J -resolved reaction cross sections (Fig. 6) nor the total integrated cross sections for $v=3$ (Fig. 7) are found to vary over this range of $p_0 \times d$. As one specific example, Fig. 9 shows the experimental ratio of state-resolved cross sections to form HF ($v=3, J=2$) at two different collision energies, $E_{\text{com}} \approx 0.42 \text{ kcal/mole}$ and $\approx 1.08 \text{ kcal/mole}$, with each cross section scaled to the value obtained for a neat H_2 expansion ($E_{\text{com}} \approx 1.74 \text{ kcal/mole}$). As will be discussed in more detail in the next section, $E_{\text{com}} \approx 0.42 \text{ kcal/mole}$ corresponds to the energetic threshold for the formation of HF($v=3, J=2$), whereas $E_{\text{com}} \approx 1.08 \text{ kcal/mole}$ is far above this threshold. This ratio might therefore be anticipated to be especially sensitive to $p_0 \times d$, if this excess rotational energy in the product HF($v=3$) arises from adiabatic reactions of ground state F atoms with uncooled $\text{H}_2(j \geq 2)$ in the expansion. By way of contrast, both of these ratios remain constant within experimental uncertainty over the full range of $p_0 \times d$ (Fig. 9), with most of the results reported in this paper conducted at 13 Torr \times cm (designated by an arrow). Thus, it is unlikely that rotationally excited $\text{H}_2(j \geq 2)$ can be responsible for the excess HF($v=3$) product state rotational energy and enhanced reactivity at low E_{com} .

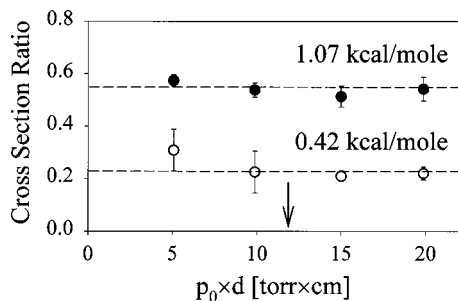


FIG. 9. Sample tests for contributions from $\text{H}_2(j \geq 2)$ levels. Shown are two cross section ratios for $\text{HF}(v=3, J=2)$, corresponding to $E_{\text{com}} \approx 0.42$ kcal/mole (open circles) and ≈ 1.07 kcal/mole (filled circles), both scaled to cross sections obtained under neat H_2 expansion conditions at $E_{\text{com}} \approx 1.74$ kcal/mole. The lower of these two collision energies (0.42 kcal/mole) is near the energetic threshold for forming $\text{HF}(v=3, J=2)$ from $\text{F} + \text{H}_2(j=1)$ and thus would be preferentially sensitive to any residual $\text{H}_2(j \geq 2)$ population in the jet expansion. However, the reaction cross sections are found to be independent (within experimental uncertainty) of $p_0 \times d$ for either (i) near the threshold or (ii) above threshold values of E_{com} , i.e., consistent with only negligible contributions from rotationally excited $\text{H}_2(j \geq 2)$. The arrow designates typical $p_0 \times d$ conditions for the rest of the work reported in this paper.

VI. THRESHOLD STUDIES

The results in the previous section clearly identify two important discrepancies between experiment and adiabatic theoretical predictions for $\text{F} + n - \text{H}_2(j=0,1)$. First of all, reactive cross sections into the $v_{\text{HF}}=3$ manifold drop off far more slowly with E_{com} than predicted from fully converged adiabatic calculations. Second, 2–3-fold more rotational energy is experimentally observed in the $\text{HF}(v=3, J)$ product manifold than theoretically predicted from $\text{F} + \text{H}_2$ calculations on the lowest adiabatic potential surface of Stark and Werner. It is important to note that the quantum calculations of Castillo *et al.* are numerically “exact” and based only on two assumptions: (i) a given *ab initio* potential energy surface, and (ii) purely adiabatic reaction dynamics on that potential surface. It is always possible that discrepancies in the cross sections and product state distributions at low E_{com} could arise simply from errors in the SW potential energy surface. Indeed, the reaction dynamics this far below the barrier are dominated by quantum tunneling, which leads one to expect exponential sensitivity to potential surface inaccuracies in the transition state barrier height, width, curvature, etc. However, as described in this section, these studies have also been performed in a regime that eliminates the possible influence of inaccuracies in the potential energy surface, and thereby permits one to focus explicitly on the role of *adiabatic* ($\text{F} + \text{H}_2$) versus *nonadiabatic* ($\text{F}^* + \text{H}_2$) contributions to the reaction dynamics.

The strategy is based on the conservation of energy, which relies only on the accurately characterized *asymptotic* properties of the $\text{F} + \text{H}_2$ potential energy surface. The exothermicity of the $\text{F} + \text{H}_2$ reaction [$\Delta E = 32.001(14)$ kcal/mole] is determined by the difference in HF and H_2 dissociation energies, which are both known to unusually high precision (± 0.014 kcal/mole) from previous spectroscopic measurements.^{89,90} This uncertainty is already much smaller than the relevant internal energy spacings in reactants or

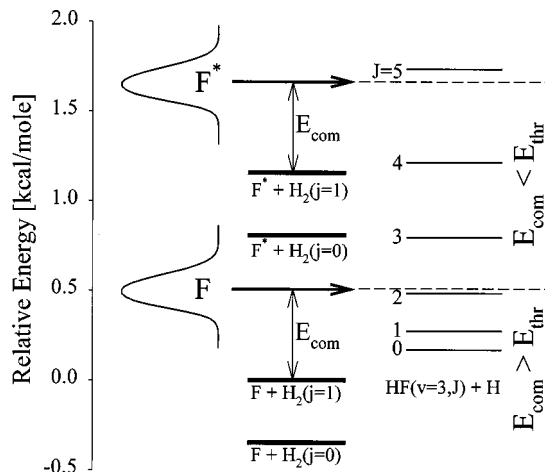


FIG. 10. Strategy for threshold studies. Shown is the energy level diagram displaying relevant combinations of the reactant and product states. The highest J state of $\text{HF}(v=3)$ that can be produced from $\text{F} + \text{H}_2(j=1)$ at $E_{\text{com}} \approx 0.5$ kcal/mole is $J \approx 2$, whereas reactions of $\text{F}^* + \text{H}_2(j=1)$ under the same conditions can produce $\text{HF}(v=3)$ up to $J \approx 5$. Thus, quantum state resolved, near threshold rotational distributions for the nascent $\text{HF}(v=3)$ products can provide a sensitive probe of the *nonadiabatic* $\text{F}^* + n - \text{H}_2$ reaction channel, based solely on (i) energy conservation and (ii) the well-known asymptotic energy levels of H_2 and HF .

products, and provides an especially good opportunity for obtaining additional dynamical insights from threshold product state studies.

For example, Fig. 10 displays the *maximum* product levels energetically accessible to F , F^* , and $\text{H}_2(j=0,1)$ reactants at $E_{\text{com}} = 0.5$ kcal/mole, i.e., where all the incident energy ($\Delta E + E_{\text{com}}$) has been converted into internal rovibrational energy of the $\text{HF}(v, J)$ product. The initial translational energy distributions of F and F^* are assumed to be identical, but with an internal energy difference equal to the spin-orbit splitting, $\Delta E_{\text{spin-orbit}} = 1.15$ kcal/mole. Since the width of the experimental E_{com} distribution (FWHM ≈ 0.2 kcal/mole at $E_{\text{com}} = 0.5$ kcal/mol) is less than or comparable to the relevant rotational energy spacings, this allows a rigorous prediction of the *highest* $\text{HF}(v=3, J)$ product state that could be formed, corresponding to zero kinetic energy recoil of the products. For example, at $E_{\text{com}} = 0.5$ kcal/mol, F can energetically access only up to $\text{HF}(v=3, J=2)$, whereas F^* at the same collision energy can produce three additional rotational levels up to $\text{HF}(v=3, J=5)$. Thus, the full quantum state resolution of the present experiment can allow one to sensitively differentiate between adiabatic and nonadiabatic reactive channels by examining the product state distributions obtained near the energetic threshold.

The results presented in Fig. 11 explicitly highlight such threshold effects. The $\text{HF}(v=3, J)$ rotational distributions obtained at a given E_{com} have been plotted as a function of threshold energy (E_{thr}), defined as the minimum collision energy required to energetically access $\text{HF}(v=3, J)$ from adiabatic reactions of $\text{F} + \text{H}_2(j=1)$. The advantage of such an abscissa is that all states with $E_{\text{thr}} \geq E_{\text{com}}$ are rigorously closed for the adiabatic $\text{F} + \text{H}_2$ reaction channel and can only be produced from nonadiabatic $\text{F}^* + \text{H}_2$ events. For compari-

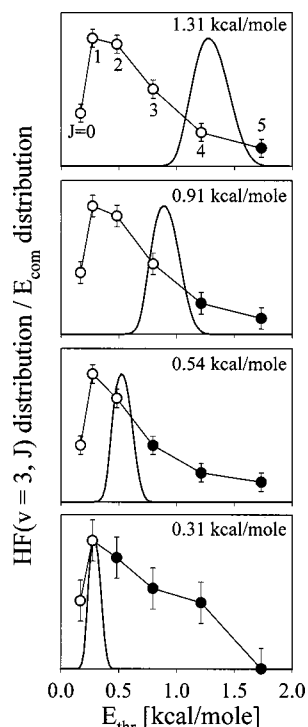


FIG. 11. Rotational distributions of HF($v=3$) products at several representative lower collision energies. The distributions are plotted as a function of the minimum E_{com} required to produce a given state of HF($v=3$) from $F+H_2(j=1)$ reactions, based on a rigorous lower limit of zero product kinetic energy recoil in the center-of-mass frame. Also shown for each case is the experimental distribution of E_{com} obtained from Monte-Carlo simulation. The shaded symbols represent states that would be energetically inaccessible via *adiabatic* $F+H_2(j=1)$ reactions and can only be produced via *nonadiabatic* reactions with F^* . Note that the net cross sections for forming HF($v=3, J$) is dropping off rapidly over this range of collision energies; for visual ease of comparison, the data for each energy have been rescaled to the same maximum value.

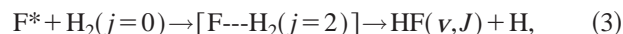
son, the distribution of center-of-mass collision energies obtained from the Monte-Carlo simulations are also shown. Figure 11 clearly shows that as the average collision energy is decreased, more HF($v=3, J$) product states are evident that are not energetically accessible to adiabatic reactions of ground state F atoms with $n-H_2$ ($j \leq 1$). For example, one, two, and three such states are clearly discernable at $E_{\text{com}} = 1.31, 0.91,$ and 0.54 kcal/mole, respectively. Finally, no product state is observed with more than $\Delta E_{\text{spin-orbit}} = 1.15$ kcal/mole beyond this adiabatic limit at each center-of-mass collision energy. In other words, all the above threshold HF(v, J) products are energetically consistent with the nonadiabatic $F^*+H_2(j=1)$ channel. In summary, these threshold results, based solely on the conservation of energy, constitute strong additional evidence for the presence of nonadiabatic reaction pathways in F^*+H_2 .

VII. DISCUSSION

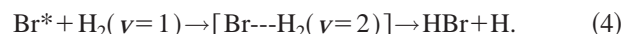
The present work provides the first experimental evidence for finite nonadiabatic reactivity between $F^*=F(^2P_{1/2})$ and H_2 , though such behavior has been long predicted by theorists. This conclusion is primarily founded on two experimental observations, both of which are made at collision energies lying *below* the reaction barrier (≈ 1.9 kcal/mole),

where the normally dominant adiabatic channel is suppressed by the reaction energetics. As the first and the most convincing experimental finding, HF(v, J) product states are detected that are energetically inaccessible from the adiabatic $F+H_2$ reaction but remain open for the corresponding F^* channel. The second confirmation comes from the results of converged QM calculations on the best available PES.^{52,84} The calculations predict vanishingly small cross sections for the $F+H_2 \rightarrow HF(v=3)+H$ reaction in the energy range of $E_{\text{com}} = 0.3-0.6$ kcal/mole, in contrast to the reaction cross sections measured experimentally. It is also demonstrated that an alternative explanation based on reactions with rotationally excited $H_2(j \geq 2)$ is much less credible, based on the small cross sections at low E_{com} , the weak dependence of these cross sections on H_2 rotational excitation, and the results of extensive experimental tests. In this section we speculate on the possible mechanism of the F^* reactivity and give some suggestions for future directions that would be required to provide a more quantitative description.

One physically appealing but clearly speculative mechanism for the F^*+H_2 reaction dynamics would involve nonadiabatic quenching of F^* followed by a reaction on the adiabatic $F+H_2$ surface in a *single collision event*. The first step in such a process could be significantly enhanced by near-resonant ($\Delta j_{H_2}=2$) electronic-to-rotational (E-R) energy exchange between F^* and H_2 ,^{60,70,72,77,78}



although some calculations⁶² predict the pure quenching processes ($\Delta j_{H_2}=0$) also to occur with comparable rates. We wish to emphasize that this is only one of many possible mechanisms⁹¹ for interpreting such a nonadiabatic event. However, there are several precedents for such behavior in the literature, at least for the heavier halogen species where spin orbit coupling effects are more significant. For example, related studies of rapid electronic-vibrational (E-V) energy transfer from spin-orbit excited $Br(^2P_{1/2})$ to $H_2(v=1)$ ⁹² demonstrate the importance of nonadiabatic (albeit highly efficient) E-V transfer in the entrance channel, followed by subsequent H atom abstraction from vibrationally excited H_2 ,

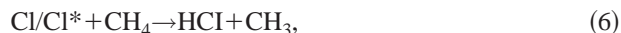


Similar evidence for nonadiabatic reaction dynamics has also been obtained in the reverse direction from studies by Polanyi and co-workers for $F+HBr \rightarrow HF(v, J) + Br$,⁹³ which demonstrated a product Br/Br^* ratio independent of the F/F^* ratio in their thermal source. This was interpreted as hydrogen abstraction to form HF(v), followed by near resonant V-E transfer from HF(v) to ground state Br atoms in the exit channel, i.e.,



These studies provide intriguing examples of efficient nonadiabatic relaxation+reaction mechanisms occurring in a *single collisional event*. Such nonadiabatic reaction processes with spin-orbit excited states could have a significant impact on the kinetics of these and other halogen/hydrogen abstraction reactions, especially for low collision energies/

temperatures where the reaction may be insufficiently energetic to proceed on the ground state adiabatic surface. For example, work by Ravishankara and Wine⁹⁴ indicates that the atmospherically important hydrogen abstraction reaction,



may, in fact, be dominated by the nonadiabatic Cl* channel at $T \leq 240$ K. Specifically, this nonadiabatic channel was invoked by Ravishankara and Wine⁹⁴ to qualitatively explain the experimentally observed nonlinearities in the Arrhenius plot as well as the rate constant sensitivity to the nature of the buffer gas. However, more recent studies from Zare's group suggest that this Arrhenius curvature might also be due to thermally excited CH bend excitation and the strong dependence of the reaction cross section on the internal vibrational state of CH₄.^{95,96} As both vibrationally activated and nonadiabatic channels are likely to contribute, a complete resolution of the relative importance of nonadiabatic versus adiabatic channels will necessitate additional work. Nevertheless, such efforts underscore that the broader issue of nonadiabatic, multisurface reaction dynamics remains one of enormous importance to chemical kinetics, a predictive understanding of which will continue to demand further theoretical and experimental investigation.

ACKNOWLEDGMENTS

This work has been supported by grants from the Air Force Office of Scientific Research and the National Science Foundation. The authors wish to express their gratitude to J. Castillo and D. Manolopoulos for providing us with unpublished results from their theoretical calculations, and to M. Alexander for providing us with potential surface data for Fig. 1.

- ¹H. Schaefer III, *J. Phys. Chem.* **89**, 5336 (1985).
- ²J. C. Polanyi and J. L. Schreiber, *Faraday Discuss. Chem. Soc.* **62**, 267 (1977).
- ³D. Manolopoulos, *J. Chem. Soc., Faraday Trans.* **93**, 673 (1997).
- ⁴J. Anderson, *Adv. Chem. Phys.* **41**, 229 (1980).
- ⁵L. D. Hess, *J. Chem. Phys.* **55**, 2466 (1971).
- ⁶K. E. Shuler, *J. Chem. Phys.* **21**, 624 (1953).
- ⁷D. Truhlar, *J. Chem. Phys.* **56**, 3189 (1972).
- ⁸J. T. Muckerman and M. D. Newton, *J. Chem. Phys.* **56**, 3191 (1972).
- ⁹R. F. Heidner III, J. F. Bott, C. E. Gardner, and J. E. Melzer, *J. Chem. Phys.* **72**, 4815 (1980).
- ¹⁰M. Ioffe, Y. Gershenzon, V. Rozenshtein, and S. Umanskii, *Chem. Phys. Lett.* **154**, 131 (1989).
- ¹¹E. Wurzberg and P. L. Houston, *J. Chem. Phys.* **72**, 4811 (1980).
- ¹²P. S. Stevens, W. H. Brune, and J. G. Anderson, *J. Phys. Chem.* **93**, 4068 (1989).
- ¹³D. M. Neumark, A. M. Wodtke, G. N. Robinson, C. C. Hayden, and Y. T. Lee, *J. Chem. Phys.* **82**, 3045 (1985).
- ¹⁴D. M. Neumark, A. M. Wodtke, G. N. Robinson, C. C. Hayden, and Y. T. Lee, *Phys. Rev. Lett.* **53**, 226 (1984).
- ¹⁵M. Faubel, L. Rusin, S. Schlemmer, F. Sondermann, U. Tappe, and J. Toennies, *J. Chem. Soc., Faraday Trans.* **89**, 1475 (1993).
- ¹⁶V. Aquilanti, R. Candori, D. Cappelletti, E. Luzzatti, and F. Pirani, *Chem. Phys.* **145**, 293 (1990).
- ¹⁷G. Dharmasena, K. Copeland, J. Young, R. Lasell, T. Phillips, G. Parker, and M. Keil, *J. Phys. Chem. A* **101**, 6429 (1997).
- ¹⁸G. Dharmasena, T. Phillips, K. Shokhirev, G. Parker, and M. Keil, *J. Chem. Phys.* **106**, 9950 (1997).
- ¹⁹J. C. Polanyi and K. B. Woodall, *J. Chem. Phys.* **57**, 1574 (1972).
- ²⁰S. Lu, C. Liu, X. Yang, K. Li, Y. Gu, and Y. Tao, *J. Chem. Phys.* **88**, 2379 (1988).
- ²¹N. Jonathan, C. M. Melliar-Smith, and D. H. Slater, *Mol. Phys.* **20**, 93 (1971).
- ²²R. D. Coombe and G. C. Pimentel, *J. Chem. Phys.* **59**, 251 (1973).
- ²³R. D. Coombe and G. C. Pimentel, *J. Chem. Phys.* **59**, 1535 (1973).
- ²⁴M. J. Berry, *J. Chem. Phys.* **59**, 6229 (1973).
- ²⁵D. M. Neumark, A. M. Wodtke, G. N. Robinson, C. C. Hayden, K. Shobatake, R. K. Sparks, T. P. Schafer, and Y. T. Lee, *J. Chem. Phys.* **82**, 3067 (1985).
- ²⁶M. Faubel, S. Schlemmer, F. Sondermann, and J. Toennies, *J. Chem. Phys.* **94**, 4676 (1991).
- ²⁷M. Faubel, L. Rusin, S. Schlemmer, F. Sondermann, U. Tappe, and J. Toennies, *J. Chem. Phys.* **101**, 2106 (1994).
- ²⁸M. Faubel, B. Martinez-Haya, L. Rusin, U. Tappe, and J. Toennies, *Chem. Phys. Lett.* **232**, 197 (1995).
- ²⁹M. Faubel, B. Martinez-Haya, L. Rusin, U. Tappe, and J. Toennies, *Z. Phys. Chem. (Leipzig)* **188**, 197 (1995).
- ³⁰M. Faubel, B. Martinez-Haya, L. Rusin, U. Tappe, J. Toennies, F. Aoz, and L. Banares, *Chem. Phys.* **207**, 227 (1996).
- ³¹M. Faubel, B. Martinez-Haya, L. Rusin, U. Tappe, and J. Toennies, *J. Phys. Chem. A* **101**, 6415 (1997).
- ³²M. Baer, M. Faubel, B. Martinez-Haya, L. Rusin, U. Tappe, and J. Toennies, *J. Chem. Phys.* **108**, 9694 (1998).
- ³³M. Ayabakan, M. Faubel, B. Martinez-Haya, L. Rusin, M. Sevryuk, U. Tappe, and J. Toennies, *Chem. Phys.* **229**, 21 (1998).
- ³⁴A. Weaver and D. M. Neumark, *Faraday Discuss. Chem. Soc.* **91**, 5 (1991).
- ³⁵A. Weaver, R. B. Metz, S. E. Bradforth, and D. M. Neumark, *J. Chem. Phys.* **93**, 5352 (1990).
- ³⁶S. Bradforth, D. Arnold, D. Neumark, and D. Manolopoulos, *J. Chem. Phys.* **99**, 6345 (1993).
- ³⁷W. B. Chapman, B. W. Blackmon, and D. J. Nesbitt, *J. Chem. Phys.* **107**, 8193 (1997).
- ³⁸W. B. Chapman, B. W. Blackmon, S. Nizkorodov, and D. J. Nesbitt, *J. Chem. Phys.* **109**, 9306 (1998).
- ³⁹K. Stark and H. Werner, *J. Chem. Phys.* **104**, 6515 (1996).
- ⁴⁰P. Knowles, K. Stark, and H. Werner, *Chem. Phys. Lett.* **185**, 555 (1991).
- ⁴¹D. G. Truhlar, B. C. Garrett, and N. C. Blais, *J. Chem. Phys.* **80**, 232 (1984).
- ⁴²T. Takayanagi and S. Sato, *Chem. Phys. Lett.* **144**, 191 (1988).
- ⁴³R. Steckler, D. G. Truhlar, and B. C. Garrett, *J. Chem. Phys.* **83**, 2870 (1985).
- ⁴⁴J. T. Muckerman, *J. Chem. Phys.* **56**, 2997 (1972).
- ⁴⁵S. L. Mielke, G. C. Lynch, D. G. Truhlar, and D. W. Schwenke, *Chem. Phys. Lett.* **213**, 10 (1993).
- ⁴⁶G. C. Lynch, P. Halvick, M. Zhao, D. G. Truhlar, Chin-hui Yu, D. J. Kouri, and D. W. Schwenke, *J. Chem. Phys.* **94**, 7150 (1991).
- ⁴⁷F. B. Brown, R. Steckler, D. W. Schwenke, D. G. Truhlar, and B. C. Garrett, *J. Chem. Phys.* **82**, 188 (1985).
- ⁴⁸F. Aoz, L. Banares, V. Herrero, V. Rabanos, K. Stark, and H. Werner, *Chem. Phys. Lett.* **223**, 215 (1994).
- ⁴⁹F. Aoz, L. Banares, V. Herrero, K. Stark, and H. Werner, *Chem. Phys. Lett.* **254**, 341 (1996).
- ⁵⁰F. Aoz, L. Banares, B. Martinez-Haya, J. Castillo, D. Manolopoulos, K. Stark, and H. Werner, *J. Phys. Chem. A* **101**, 6403 (1997).
- ⁵¹J. F. Castillo, B. Hartke, H. J. Werner, F. J. Aoz, L. Banares, and B. Martinez-Haya, *J. Chem. Phys.* **109**, 7224 (1998).
- ⁵²J. Castillo, D. Manolopoulos, K. Stark, and H. Werner, *J. Chem. Phys.* **104**, 6531 (1996).
- ⁵³E. Rosenman and A. Persky, *Chem. Phys.* **195**, 291 (1995).
- ⁵⁴B. Hartke and H. Werner, *Chem. Phys. Lett.* **280**, 430 (1997).
- ⁵⁵D. Manolopoulos, K. Stark, H. Werner, D. Arnold, S. Bradforth, and D. Neumark, *Science* **262**, 1852 (1993).
- ⁵⁶G. A. Laguna and W. H. U. Beattie, *Chem. Phys. Lett.* **88**, 439 (1982).
- ⁵⁷A. C. Stanton and C. E. Kolb, *J. Chem. Phys.* **72**, 6637 (1980).
- ⁵⁸M. Alexander, H. Werner, and D. Manolopoulos, *J. Chem. Phys.* **109**, 5710 (1998).
- ⁵⁹G. D. Billing, L. Y. Rusin, and M. B. Sevryuk, *J. Chem. Phys.* **103**, 2482 (1995).
- ⁶⁰D. E. Fitz and D. J. Kouri, *J. Chem. Phys.* **74**, 3933 (1981).
- ⁶¹M. Gilbert and M. Baer, *J. Phys. Chem.* **98**, 12 822 (1994).
- ⁶²M. Gilbert and M. Baer, *J. Phys. Chem.* **99**, 15 748 (1995).
- ⁶³A. Komornicki, T. F. George, and K. Morokuma, *J. Chem. Phys.* **65**, 4312 (1976).

- ⁶⁴A. Komornicki, T. F. George, and K. Morokuma, *J. Chem. Phys.* **67**, 5012 (1977).
- ⁶⁵I. Last, M. Baer, I. H. Zimmerman, and T. F. George, *Chem. Phys. Lett.* **101**, 163 (1983).
- ⁶⁶B. Lepetit, J. M. Launay, and M. Le Dourneuf, *Chem. Phys.* **106**, 111 (1986).
- ⁶⁷C. W. McCurdy, H. D. Meyer, and W. H. Miller, *J. Chem. Phys.* **70**, 3177 (1979).
- ⁶⁸J. F. McNutt and R. E. Wyatt, *Chem. Phys.* **58**, 423 (1981).
- ⁶⁹F. Reberstrost and W. A. Lester, Jr., *J. Chem. Phys.* **63**, 3737 (1975).
- ⁷⁰F. Reberstrost and W. A. Lester, Jr., *J. Chem. Phys.* **64**, 4223 (1976).
- ⁷¹F. Reberstrost and W. A. Lester, Jr., *J. Chem. Phys.* **64**, 3879 (1976).
- ⁷²F. Reberstrost and W. A. Lester, Jr., *J. Chem. Phys.* **67**, 3367 (1977).
- ⁷³F. Reberstrost, *Chem. Phys. Lett.* **58**, 18 (1978).
- ⁷⁴L. D. Thomas, W. A. Lester, Jr., and F. Reberstrost, *J. Chem. Phys.* **69**, 5489 (1978).
- ⁷⁵J. C. Tully, *J. Chem. Phys.* **59**, 5122 (1973).
- ⁷⁶J. C. Tully, *J. Chem. Phys.* **60**, 3042 (1974).
- ⁷⁷R. E. Wyatt, *Chem. Phys. Lett.* **63**, 503 (1979).
- ⁷⁸R. E. Wyatt and R. B. Walker, *J. Chem. Phys.* **70**, 1501 (1979).
- ⁷⁹I. H. Zimmerman, M. Baer, and T. F. George, *J. Chem. Phys.* **71**, 4132 (1979).
- ⁸⁰S. A. Nizkorodov, W. W. Harper, and D. J. Nesbitt, *Faraday Discuss. Chem. Soc.* (in press).
- ⁸¹D. Proch and T. Trickl, *Rev. Sci. Instrum.* **60**, 713 (1989).
- ⁸²S. A. Nizkorodov, W. W. Harper, and D. J. Nesbitt (manuscript in preparation).
- ⁸³E. Arunan, D. W. Setser, and J. F. Ogilvie, *J. Chem. Phys.* **97**, 1734 (1992).
- ⁸⁴J. Castillo and D. Manolopoulos (private communication).
- ⁸⁵J. E. Pollard, D. J. Trevor, Y. T. Lee, and D. A. Shirley, *J. Chem. Phys.* **77**, 4818 (1982).
- ⁸⁶P. Huber-Walchli and J. W. Nibler, *J. Chem. Phys.* **76**, 273 (1982).
- ⁸⁷R. J. Gallagher and J. B. Fenn, *J. Chem. Phys.* **60**, 3492 (1974).
- ⁸⁸K. Dharmasena, J. Jefferies, G. Mu, J. Young, B. Bergeron, R. Littell, and N. Shafer-Ray, *Rev. Sci. Instrum.* **69**, 2888 (1998).
- ⁸⁹W. C. Stwalley, *Chem. Phys. Lett.* **6**, 241 (1970).
- ⁹⁰W. T. Zemke, W. C. Stwalley, J. A. Coxon, and P. G. Hajigeorgiou, *Chem. Phys. Lett.* **177**, 412 (1991).
- ⁹¹G. M. Sweeney and K. G. McKendrick, *J. Chem. Phys.* **106**, 9182 (1997).
- ⁹²D. J. Nesbitt and S. R. Leone, *J. Chem. Phys.* **73**, 6182 (1980).
- ⁹³D. Brandt and J. C. Polanyi, *Chem. Phys.* **45**, 65 (1980).
- ⁹⁴A. R. Ravishankara and P. H. Wine, *J. Chem. Phys.* **72**, 25 (1980).
- ⁹⁵S. A. Kandel and R. N. Zare, *J. Chem. Phys.* **109**, 9719 (1998).
- ⁹⁶W. R. Simpson, T. P. Rakitzis, S. A. Kandel, A. J. Orr-Ewing, and R. N. Zare, *J. Chem. Phys.* **103**, 7313 (1995).